Available online at www.sciencedirect.com
ScienceDirect
Pattern Recognition 40 (2007) 141–153
PATTERN RECOGNITION
THE JOURNAL OF THE PATTERN RECOGNITION SOCIETY
www.elsevier.com/locate/patcog

Shape recognition using eigenvalues of the Dirichlet Laplacian

M.A. Khabou[a], L. Hermi[b,*], M.B.H. Rhouma[c]

[a]*Electrical & Computer Engineering Department, University of West Florida, 11000 University Parkway Pensacola, FL 32514, USA*
[b]*Department of Mathematics, University of Arizona, Tucson, AZ 85721-0089, USA*
[c]*Department of Mathematics and Statistics, Sultan Qaboos University, Alkhod 123, Muscat, Oman*

Received 9 June 2005; received in revised form 20 December 2005; accepted 3 January 2006

Abstract

The eigenvalues of the Dirichlet Laplacian are used to generate three different sets of features for shape recognition and classification in binary images. The generated features are rotation-, translation-, and size-invariant. The features are also shown to be tolerant of noise and boundary deformation. These features are used to classify hand-drawn, synthetic, and natural shapes with correct classification rates ranging from 88.9% to 99.2%. The classification was done using few features (only two features in some cases) and simple feedforward neural networks or minimum Euclidian distance.

Keywords: Shape recognition; Eigenvalues; Laplacian; Fixed membrane problem; Dirichlet boundary condition; Neural networks

1. Introduction

It is very possible that two or more persons have similar silhouettes. But what is the probability that two persons chosen randomly have the same silhouette? The answer is practically zero, and thus seeing the silhouette of an acquaintance in the dark one can in general tell who that person is. It was also proven mathematically that two differently shaped drums can give similar sounds. But what is the probability that two randomly chosen drums give the same sound? The answer is again practically zero, and thus the following question becomes natural: knowing the sound of a drum, determined by the eigenvalues of the Dirichlet Laplacian (that is the frequencies of the fixed membrane assuming the shape of this drum), can one narrow down its shape? The purpose of this paper is to show that the eigenvalues of the Dirichlet Laplacian can indeed be used as a reliable feature descriptor for shapes.

Shape analysis is a key component in object recognition, matching, registration and analysis. A shape description method generates a feature vector that will (or at least attempt to) uniquely characterize the silhouette of the object. This feature vector should, in many cases, be translation-, rotation-, and size-invariant. Depending on the application at hand, a certain level of robustness and tolerance to shape deformation and noise is also required. Shape recognition has greatly benefited from the classical theories of human visual perception such as [1–4] and more modern ones [5–9]. Those theories have inspired several methods for shape analysis that can be classified in several ways [10]. For example, a shape recognition technique is either numeric or non-numeric, depending on the nature of the output of the shape analysis. While most methods produce a vector feature to describe the shape, a few methods such as the medial axis transform (MAT) [11] produces another image instead. A shape recognition technique can also be classified as either information preserving or non-preserving. One can recover the shape of an information preserving method, while a non-preserving method may only allow for a partial recovery of the actual shape. However, by far the most popular classification [12] of shape techniques divides the different methods into two groups: boundary methods and global methods. Boundary methods treat the boundary or exterior points of the shape,

* Corresponding author. Tel.: +1 520 481 4830; fax: +1 520 621 8322.
E-mail addresses: mkhabou@uwf.edu (M.A. Khabou), hermi@math.arizona.edu (L. Hermi), rhouma@squ.edu.om (M.B.H. Rhouma).

0031-3203/$30.00
doi:10.1016/j.patcog.2006.01.002

while global methods deal with the interior points of the object.

There is no clear consensus which method or category of methods works best. Each method seems to give good results in some applications and fail in some others or in presence of noise. The method that we present in this paper is a numerical, non-preserving global method that attempts to use the ratios of eigenvalues of the Dirichlet Laplacian operator of a certain shape as the feature vector.

Following a brief mathematical overview in the next section relating shapes to eigenvalues of the Dirichlet Laplacian, we describe in Section 3 how we compute the eigenvalues of a given shape. In Section 4, we explain how we use these eigenvalues to generate three different features sets that are rotation-, translation-, and size-invariant and we probe their stability, their tolerance to noise and boundary deformation, and their ability to separate shapes from different classes. In Section 5, we present the results of our shape recognition experiments.

2. Eigenvalues of the Dirichlet Laplacian

"Can one hear the shape of a drum?" is a colorful old question asked by Kac [13] (see also the equally entertaining [14]) in a much-quoted 1966 paper and answered relatively recently by Gordon et al. [15]. Unfortunately the answer is negative, which means that in general, knowing the key modes of vibration of a drum is not enough to determine its shape. However, much can be said in the affirmative for some cases. That is, with additional restrictions on the type of drum, one can hear its shape. Mathematically speaking, given a bounded planar domain Ω, the sequence of eigenvalues

$$0 < \lambda_1 < \lambda_2 \leqslant \lambda_3 \leqslant \cdots \leqslant \lambda_k \leqslant \cdots \to \infty \tag{1}$$

of the partial differential equation

$$\Delta u + \lambda u = 0 \quad \text{in } \Omega \tag{2}$$

with Dirichlet boundary condition $u = 0$ on its boundary $\partial\Omega$ is not enough to tell us what is exactly the domain Ω. Here, $\Delta = \partial^2/\partial x^2 + \partial^2/\partial y^2$ is the Laplacian operator. Perhaps this is the reason why eigenvalues of the Dirichlet Laplacian did not find their way to shape recognition except only recently [16] despite the large body of engineering and mathematical literature on the computational aspects of the fixed membrane problem. See Refs. [17–34] to list just a few.

Since the celebrated work of Payne–Pólya–Weinberger [35] (see also Refs. [37,38]) we now know a variety of *universal inequalities* for the eigenvalues problem (2) which do not depend explicitly on the shape or size of the underlying domain. For instance

$$\lambda_{m+1} - \lambda_m \leqslant 2\frac{\sum_{i=1}^{m} \lambda_i}{m} \quad \text{for } m = 1, 2, 3, \ldots, \tag{3}$$

which was proved back in 1956. Note that as a result of the natural ordering of the eigenvalues (1) and (3) one can conclude that

$$\frac{\lambda_{m+1}}{\lambda_m} \leqslant 3 \quad \text{for } m = 1, 2, 3, \ldots. \tag{4}$$

There is also the inequality of Hile and Protter [39] which states

$$\sum_{i=1}^{m} \frac{\lambda_i}{\lambda_{m+1} - \lambda_i} \geqslant \frac{m}{2}. \tag{5}$$

These two inequalities were strengthened in 1991 by Yang [40] (see also Refs. [37,38]) to

$$\sum_{i=1}^{m} (\lambda_{m+1} - \lambda_i)^2 \leqslant 2\sum_{i=1}^{m} \lambda_i(\lambda_{m+1} - \lambda_i). \tag{6}$$

A weaker, but explicit, form of this last inequality, still stronger than both (3) and (5) states

$$\lambda_{k+1} \leqslant 3\frac{1}{k}\sum_{j=1}^{k} \lambda_j. \tag{7}$$

These eigenvalues also exhibit a variety of *isoperimetric* properties. For instance, the Faber–Krahn inequality [41] states

$$\lambda_1 \geqslant \frac{\pi^2 j_{0,1}^2}{|\Omega|}, \tag{8}$$

where $j_{0,1} = 2.4048\ldots$ is the first zero of the Bessel function $J_0(x)$ [42], and $|\Omega|$ is the area of the vibrating drum. There is also the beautiful improvement of Eq. (4) (for $m = 1$) by Ashbaugh–Benguria [37,38,43],

$$\frac{\lambda_2}{\lambda_1} \leqslant \frac{j_{1,1}^2}{j_{0,1}^2} = 2.53873\ldots. \tag{9}$$

Here $j_{1,1} = 3.83171\ldots$ is the first zero of the Bessel function $J_1(x)$. Equality is attained in Eqs. (8) and (9) if and only if the underlying domain Ω is a disk. These inequalities are called *isoperimetric* in parallel with the classical property of the circle being the figure assuming the largest area for a fixed perimeter. Stability results for these inequalities were proved by Melas [44]. In the colorful language of Kac and followers, the result of Melas states that one can hear a convex drum if its first eigenvalue, or ratio of the first and second eigenvalues, are close to those of a disk. In this case, the drum must be close to a disk.

Explicit formulas to compute the eigenvalues of simple particular shapes do exist. For example, the eigenvalues of a square with side L are given by

$$\lambda_{nm} = \frac{\pi^2}{L^2}(n^2 + m^2) \quad \text{for } n, m = 0, 1, 2, \ldots. \tag{10}$$

For instance, when $L=\pi$, the first few eigenvalues (counting multiplicity) are: 2, 5, 5, 8, 10, 10, 13, 13, 17, ... For more complex shapes, numerical approximation methods are used. The inequalities listed above can be used to check the correctness of the approximation. We describe the method we used to compute the eigenvalues of a certain shape in the next section.

A key property of the eigenvalues of the Dirichlet Laplacian is called *domain monotinicity*. It states the following:

If $\Omega_1 \subset \Omega_2$ then $\lambda_k(\Omega_1) \geqslant \lambda_k(\Omega_2)$.

In physical terms, this means a smaller domain gives rise to a higher pitch.

Another key property (see Chapter 5 of Ref. [45]) states the following:

$$\lambda_k(\alpha\Omega) = \frac{\lambda_k(\Omega)}{\alpha^2}, \tag{11}$$

where $\alpha > 0$ and $\alpha\Omega$ is a scaling by α of the underlying domain Ω. This means that

$$\frac{\lambda_k(\alpha\Omega)}{\lambda_m(\alpha\Omega)} = \frac{\lambda_k(\Omega)}{\lambda_m(\Omega)}. \tag{12}$$

It is also well-known that the eigenvalues of the Dirichlet Laplacian are preserved if the underlying domain Ω is translated or rotated (for a proof of this property see Refs. [16,45]). These properties make eigenvalues very useful as features in recognizing shapes of different sizes and orientations. For example, Zuliani et al. [16] used eigenvalue-based curve descriptors in a retrieval system from a multi-view curve dataset consisting of 40 curves imaged under 14 different points of view. Their system had a relatively high recall rate (86%) and was shown to be tolerant of some curve distortion. Their retrieval system was very simple using the Euclidean distance as the similarity measure.

3. Computation of the eigenvalues

The 1950s saw also a confluence of theoretical studies of finite difference methods (FDM) for estimating the eigenvalues of Eq. (2). The oldest and most natural finite difference scheme [30] is to replace Eq. (2) with the recursive formula

$$\frac{u_{i+1,j} + u_{i,j+1} + u_{i-1,j} + u_{i,j-1} - 4u_{ij}}{h^2} = -\lambda u_{ij}. \tag{13}$$

Here the domain is cut into squares of side h, u_{ij} is the value of the eigenfunction corresponding to λ at the lattice point (ih, jh). This scheme can be put in the form [16]

$$\mathscr{L}u = \lambda u,$$

where

$$\mathscr{L} = \frac{1}{h^2}\begin{bmatrix} A & I_n & 0 & \cdots & 0 \\ I_n & A & I_n & \cdots & 0 \\ \vdots & \vdots & \ddots & \vdots & \vdots \\ 0 & 0 & 0 & \cdots & A \end{bmatrix}_{n^2\times n^2} \quad \text{and}$$

$$A = \begin{bmatrix} -4 & 1 & 0 & \cdots & 0 \\ 1 & -4 & 1 & \cdots & 0 \\ 0 & 1 & -4 & \cdots & 0 \\ \vdots & \vdots & \ddots & \vdots & \vdots \\ 0 & 0 & 0 & \cdots & -4 \end{bmatrix}_{n\times n}.$$

Here, n is inversely proportional to h and accounts for the size of the domain Ω. The eigenvalues $\lambda'_1, \lambda'_2, \ldots$ of this finite dimensional problem provide, in general [18,19,29], lower bounds for $\lambda_1, \lambda_2, \ldots$ (respectively).

Two alternative schemes were also developed by Pólya [29,30,33,34]. These schemes take the general form

$$\mathscr{L}_{ij}u = \lambda\mathscr{R}_{ij}u.$$

In the first scheme, $\mathscr{L}_{ij}u$ and $R_{ij}u$ are given by

$$\begin{aligned} \mathscr{L}_{ij}u &= \frac{1}{h^2}(u_{i+1,j} + u_{i,j+1} + u_{i-1,j} + u_{i,j-1} - 4u_{ij}), \\ \mathscr{R}_{ij}u &= -\tfrac{1}{12}(6u_{ij} + u_{i+1,j} + u_{i,j+1} + u_{i-1,j} \\ &\quad + u_{i-1,j-1} + u_{i,j-1}). \end{aligned} \tag{14}$$

In the second scheme, $\mathscr{L}_{ij}u$ and $\mathscr{R}_{ij}u$ take the forms,

$$\begin{aligned} \mathscr{L}_{ij}u &= \frac{1}{3h^2}(u_{i+1,j} + u_{i,j+1} + u_{i-1,j} + u_{i,j-1} - 8u_{ij}), \\ \mathscr{R}_{ij}u &= -\tfrac{1}{36}(16u_{ij} + 4_{ui+1,j} + 4u_{i,j+1} + 4u_{i-1,j} \\ &\quad + 4u_{i,j-1} + u_{i+1,j+1} + u_{i+1,j-1} \\ &\quad + u_{i-1,j+1} + u_{i-1,j-1}). \end{aligned} \tag{15}$$

The schemes described by Eqs. (14) and (15) yield upper bounds for $\lambda_1, \lambda_2, \ldots$. However, as $h \to 0$, the eigenvalues approximated using methods (13), (14) and (15) converge to the theoretical ones (see Table 1 for the case of a square). Method (13) is computationally simpler and faster and hence was chosen for our purposes.

There are alternative schemes using the finite elements method (FEM) originating in the work of Courant in the 1940s and others [25,31,46]. Another well elaborate scheme called the method of intermediate problems of Aronszajn and Weinstein provides different estimates for these eigenvalues (see Ref. [47] where many numerical examples are exhibited). The works of Kuttler and Sigillito, together and with other co-authors, provide good reviews of the use of the difference method in determining eigenvalues [25,27,28]. The books [32,48,49] provide comprehensive references for the finite-difference method and its many applications. We hope to use some of these schemes for the purposes of shape recognition in future work.

Table 1
Comparing the first nine eigenvalues of a square of side $L = \pi$ using methods (13), (14), and (15)

	Exact	5×5 mesh			10×10 mesh			20×20 mesh		
		(13)	(14)	(15)	(13)	(14)	(15)	(13)	(14)	(15)
λ_1	2	1.95	2.15	2.05	1.99	2.04	2.01	2.00	2.01	2.00
λ_2	5	4.62	5.80	5.40	4.89	5.24	5.12	4.97	5.07	5.03
λ_3	5	4.62	5.81	5.40	4.89	5.24	5.12	4.97	5.07	5.03
λ_4	8	7.30	10.33	8.75	7.78	8.69	8.22	7.94	8.19	8.06
λ_5	10	8.27	12.84	11.97	9.46	10.85	10.57	9.85	10.23	10.15
λ_6	10	8.27	12.84	11.97	9.46	10.86	10.57	9.85	10.24	10.15
λ_7	13	10.94	18.76	15.32	12.36	14.73	13.67	12.82	13.48	13.18
λ_8	13	10.94	18.76	15.32	12.36	14.75	13.67	12.82	13.48	13.18
λ_9	17	11.92	23.96	21.89	15.33	19.30	18.81	16.53	17.64	17.48

4. Feature generation and evaluation

For a given binary image Ω, we consider extracting three sets of features based on the eigenvalues described above. They are defined by

$$F_1(\Omega) \equiv \left\{ \left(\frac{\lambda_1}{\lambda_2}, \frac{\lambda_1}{\lambda_3}, \frac{\lambda_1}{\lambda_4}, \ldots, \frac{\lambda_1}{\lambda_n} \right) \right\}, \tag{16}$$

$$F_2(\Omega) \equiv \left\{ \left(\frac{\lambda_1}{\lambda_2}, \frac{\lambda_2}{\lambda_3}, \frac{\lambda_3}{\lambda_4}, \ldots, \frac{\lambda_{n-1}}{\lambda_n} \right) \right\}, \tag{17}$$

and

$$F_3(\Omega) \equiv \left\{ \left(\frac{\lambda_1}{\lambda_2} - \frac{d_1}{d_2}, \frac{\lambda_1}{\lambda_3} - \frac{d_1}{d_3}, \frac{\lambda_1}{\lambda_4} - \frac{d_1}{d_4}, \ldots, \frac{\lambda_1}{\lambda_n} - \frac{d_1}{d_n} \right) \right\}, \tag{18}$$

where n counts the number of features we wish to use for our recognition scheme, and $d_1 < d_2 \leqslant d_3 \leqslant \cdots \leqslant d_n$ are the first n eigenvalues (counting multiplicity) of a disk. All three feature sets are obviously size-invariant by virtue of Eq. (12). The F_1 features are the same as those used by Zuliani et al. [16] in their retrieval system. The values in $F_1(\Omega)$ and $F_2(\Omega)$ are in the unit cube, and those in $F_3(\Omega)$ are between -1 and 1—a useful range when using neural networks. This latter descriptor is a good measure of the deviation of Ω from a disk. The optimal number of features n depends on the problem being addressed and is determined experimentally.

To test the consistency of these feature sets for a given image class, their tolerance to noise and change in boundary shape, and their capability to separate different image classes, we conducted a set of experiments with simple computer generated images. We report on the results of these experiments in the following subsections.

4.1. Consistency and stability of features

A good feature set should be consistent for a given class. A particular feature should have a fairly constant value for all images from a particular class. The consistency of a feature can be measured using its standard deviation from the mean for that image class. To test the consistency of the three feature sets we are using, we conducted two sets of experiments. A description of these experiments follows.

4.1.1. Simple shapes experiment

We generated 100 binary images each from five classes: disks, ellipses, rectangles, triangles, and squares. These images had random sizes and orientations (see Figs. 1(a)–5(a)). Note that some images were so small that it is hard, even for a human, to distinguish them apart. The eigenvalues of these images were computed and $n = 20$ features from each set F_1, F_2, and F_3 were generated. For each feature descriptor, the average and standard deviation over the 100 images from each class were computed and are shown in Figs. 1(b)–5(b). Note that, in all cases, the F_2-curve is never below $1/2.53873\ldots \approx 0.4$—this is, of course, a reflection of the theoretical result (4) (see also Eq. (9)). As can be seen from these figures, the standard deviations for all feature sets are fairly small. This is a good indicator of the stability and consistency of the feature sets with regard to size and orientation. The small variations are mainly due to the digital nature of the images (pixels) and to the rounding errors in the calculation/approximation of the eigenvalues. Some of the shapes appear to have, on average, similar feature values (for example, the ellipses' and squares' features shown in Figs. 1(b) and 2(b), respectively). However, there was a consistent small difference between the two feature sets that allowed even a simple neural network classifier (described later in this section) to distinguish them apart more than 99% of the time.

4.1.2. Petal images experiment

We generated a number of binary images using the polar equation

$$r = a + \varepsilon \cos\theta + \cos n\theta. \tag{19}$$

The value of θ varies from 0 to 2π. This equation generates images that look like flowers with n petals. The value of a determines the size of the interior of the image and ε is a number between -1 and 1 that acts as a perturbation

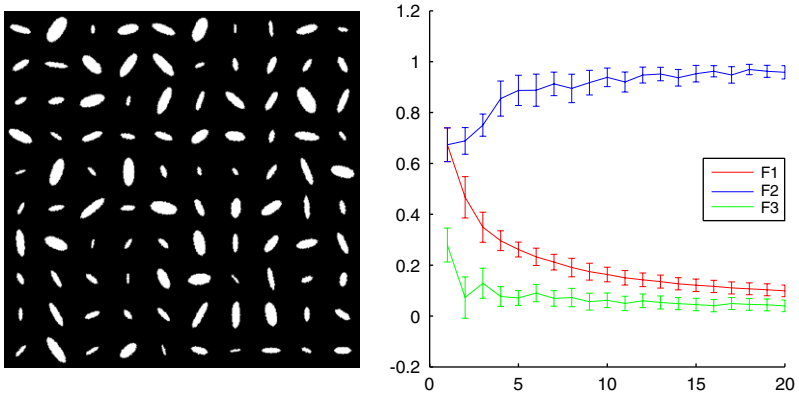

(a) (b)

Fig. 1. (a) Images of 100 random ellipses and (b) the average and standard deviation of the first 20 features from F_1, F_2, and F_3.

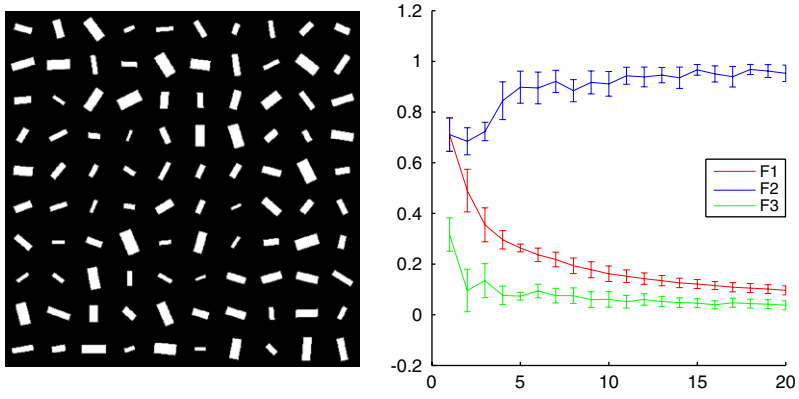

(a) (b)

Fig. 2. (a) Images of 100 random rectangles and (b) the average and standard deviation of the first 20 features from F_1, F_2, and F_3.

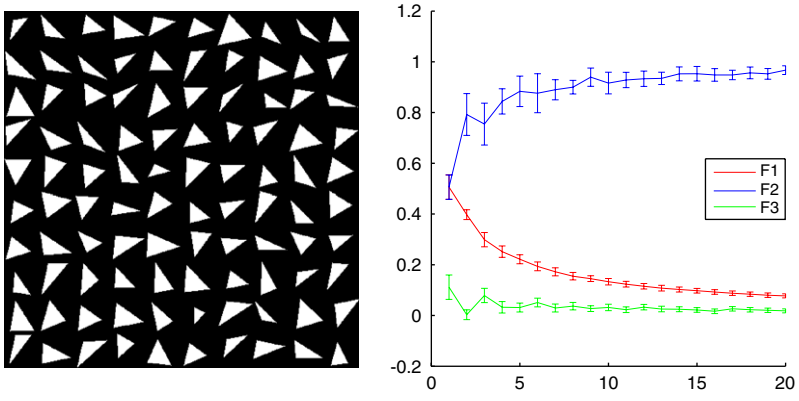

(a) (b)

Fig. 3. (a) Images of 100 random triangles and (b) the average and standard deviation of the first 20 features from F_1, F_2, and F_3.

parameter and affects the appearance of the petals. When $\varepsilon = 0$, the petals are perfectly identical. As ε deviates from zero, some of the petals get smaller and the others get bigger. However, the number of petals does not change as long as $-1 \leqslant \varepsilon \leqslant 1$. When ε is outside this range, the number of petals changes and the shape of the generated image is drastically altered. For this experiment we generated two sets of 100 images each. The first set of images was generated by setting $a = 2$, $n = 4$, and letting ε vary from 0 to 0.99. The second set of images were generated by setting $a = 2$, $n = 5$, and

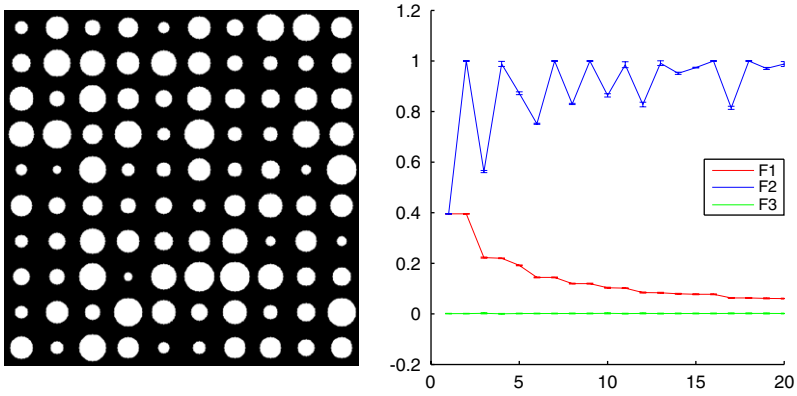

Fig. 4. (a) Images of 100 random disks and (b) the average and standard deviation of the first 20 features from F_1, F_2, and F_3.

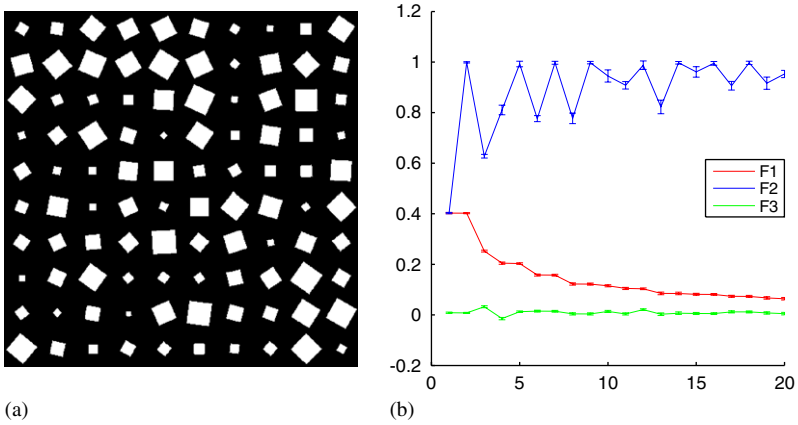

Fig. 5. (a) Images of 100 random squares and (b) the average and standard deviation of the first 20 features from F_1, F_2, and F_3.

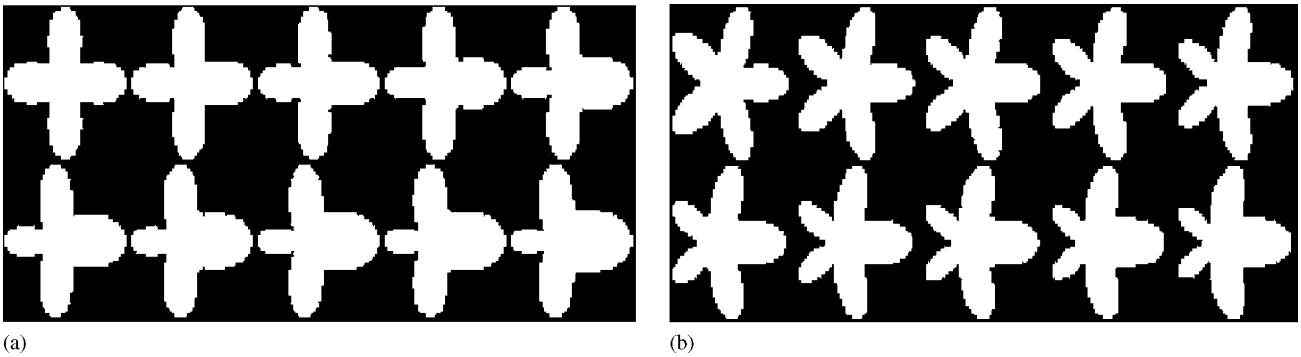

Fig. 6. Sample images of the (a) 4-petal and (b) 5-petal images.

letting ε vary from 0 to 0.99. Sample images are shown in Fig. 6. For each image in these two sets, we computed its F_1, F_2, and F_3 features. The first five features from each feature set are plotted in Figs. 7–8. Note that all features stayed fairly constant even though the shapes were deformed as ε changed from 0 to 0.99. This is a good indication of the stability and consistency of these features under this sort of boundary deformation. That the first feature in Figs. 7(b) and 8(b) is above 0.4 is again a reflection of the Theorem of Ashbaugh–Benguria (9) [43]. That the higher features in Figs. 7(b) and 8(b) are above 0.4 is a standing conjecture of Payne–Pólya–Weinberger [35].

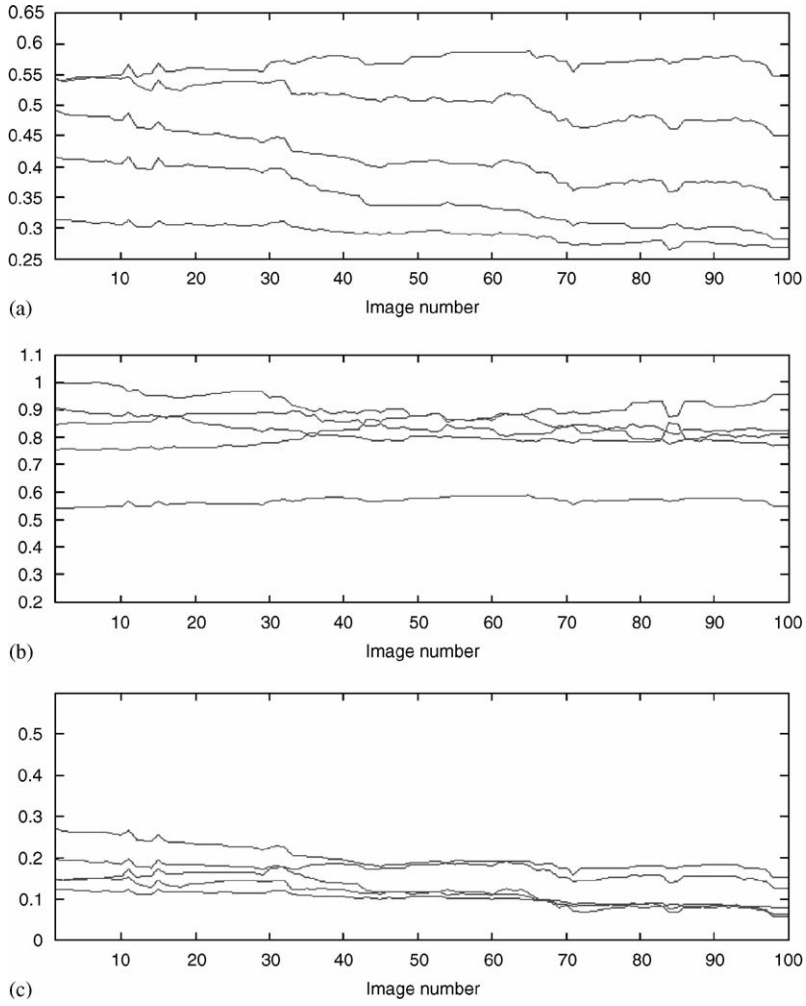

Fig. 7. Plot of first five (a) F_1, (b) F_2, and (c) F_3 features for all 4-petal images.

4.2. Tolerance to noise

Since eigenvalues are somehow affected by variation in the boundary of an input image, we wanted to quickly investigate the tolerance of the feature sets to noise on the boundary. We randomly corrupted 20% of the boundary pixels by either adding or deleting pixels at those locations. These boundary alterations are more visible in small images. We computed the features of these noisy images and compared their values to those of the original uncorrupted images. The features of the noisy images were almost identical to those of the original images. For example, Fig. 9 shows the average F_1 features for the original and noisy images for the five simple shape classes described earlier. As can clearly be seen, there is little difference between the features in both cases. This is a good indicator of the feature sets tolerance to boundary noise.

4.3. Class separation capability

A good feature set should react differently to images from different classes producing feature vectors that are very different from class to class. Another desirable property of a feature set is that only "few" features are needed to discriminate between classes. Using fewer features allows the design of a simpler and faster classification system. Obviously, the number of features needed in a particular classification problem depends on how many classes there are and how complex the classes are.

For example, to separate the 4-petal images from the 5-petal images, we need to use *only the first* feature from the F_1 set. Fig. 10 shows that this one feature is sufficient to separate the 4-petal images from the 5-petal images despite the variability in the shape of the images in each class. Note that the first feature for 4- and 5-petal images is again above 0.4 as predicted by the Theorem of Ashbaugh–Benguria (9) [43].

We conducted another experiment to investigate how many F_1, F_2, and F_3 features are necessary to separate the computer-generated images of disks, squares, rectangles, triangles and ellipses that we mentioned earlier. We trained simple feedforward neural networks with one hidden layer using $n = 4, 8, 12, 16$, and 20 features to classify images

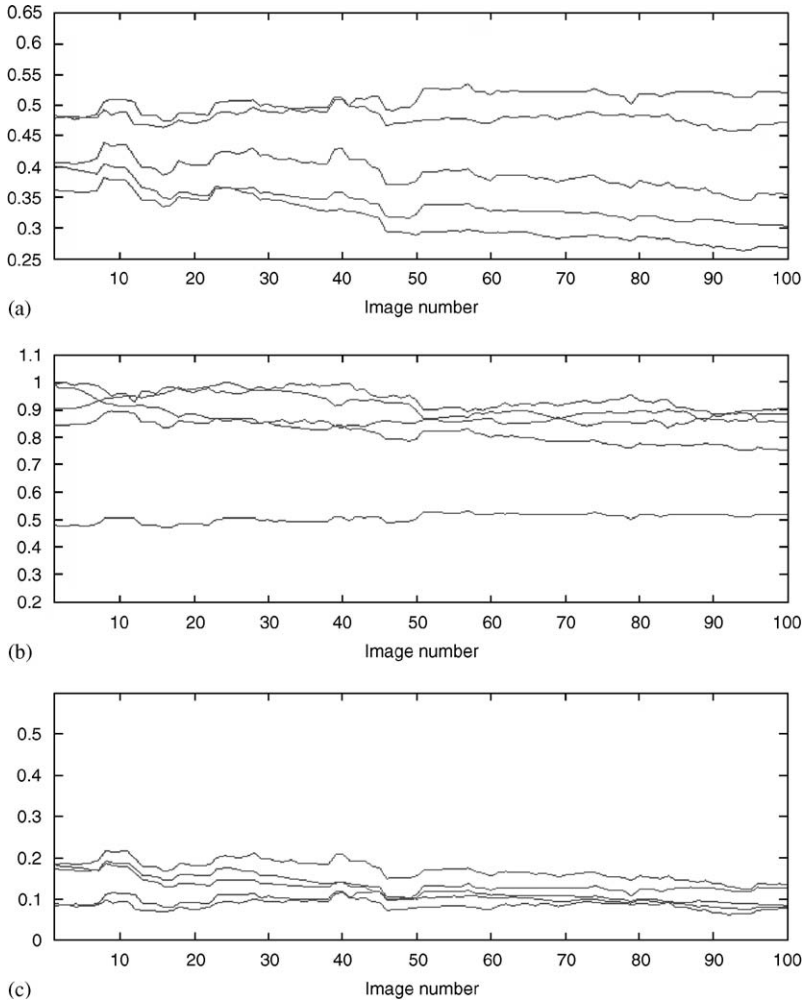

Fig. 8. Plot of first five (a) F_1, (b) F_2, and (c) F_3 features for all 5-petal images.

from these five classes. The neural networks were trained using half of the images (250) in the dataset. The other half is divided equally between validation and test sets (125 each). Table 2 summarizes the results of these experiments. As can be seen from the table, we needed only $n = 8$ features from the F_1 set to attain a 99.2% correct classification rate. For the same recognition rate, one would need $n = 20$ features from the F_2 set. The best recognition rate for the F_3 set was 98.4%, obtained using $n = 16$ features. Many of the misclassified images were very small images that are hard to classify even by a human.

5. Shape recognition experiments

In this section, we report the results of three shape recognition experiments we conducted using three different data sets. The results will show the effectiveness, robustness, and noise tolerance of the three feature sets. The three data sets we used consisted of hand-drawn shapes, computer-generated n-petal images, and images of different tree leaves. A description of these experiments follows.

5.1. Hand-drawn shapes

Forty disks, triangles, rectangles, ellipses, and squares of different sizes and orientations (200 images total) were hand drawn and scanned into the computer. Samples are shown in Fig. 11.

As can be seen from these samples, the boundaries of these shapes are noisy and irregular. Also, some of the ellipses look similar to the circles and vice versa. The three sets of features for each image were calculated. We used the neural nets we trained on the *computer-generated* shapes (described earlier) to classify these hand-drawn images. Table 3 summarizes the correct classification rates on the test set for the different networks/feature sets we used. As can be seen from the table, we were able to attain a good classification rate (94% average) based on all features sets and using a relatively small number of feature (only eight in the F_3 case). This shows that the feature sets were robust/stable enough to tolerate a relatively high degree of noise and/or deformation on the image boundary. This also shows the class separation capability of these feature sets.

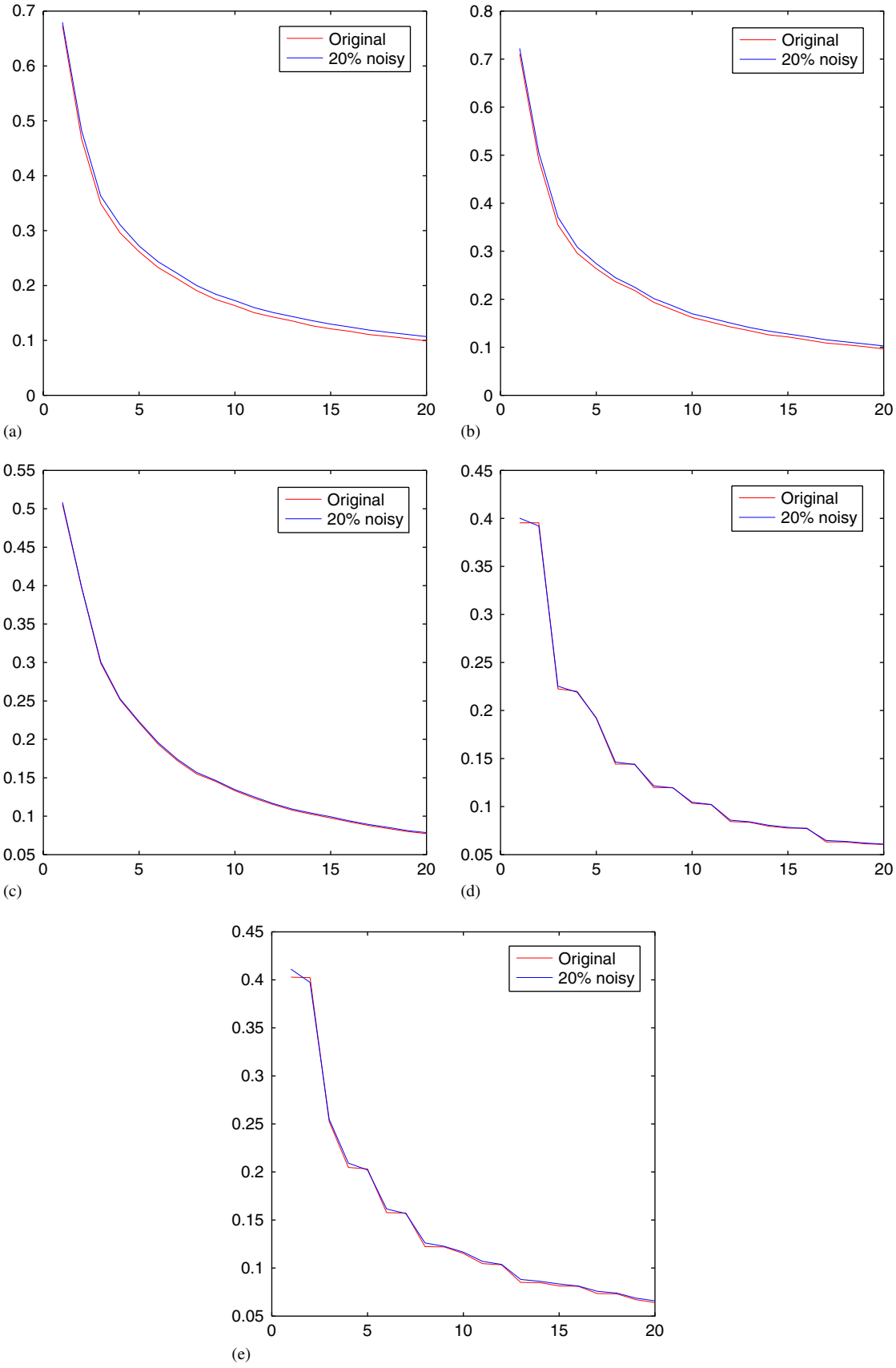

Fig. 9. Noise effects for F_1 features for (a) ellipses, (b) rectangles, (c) triangles, (d) disks, and (e) squares.

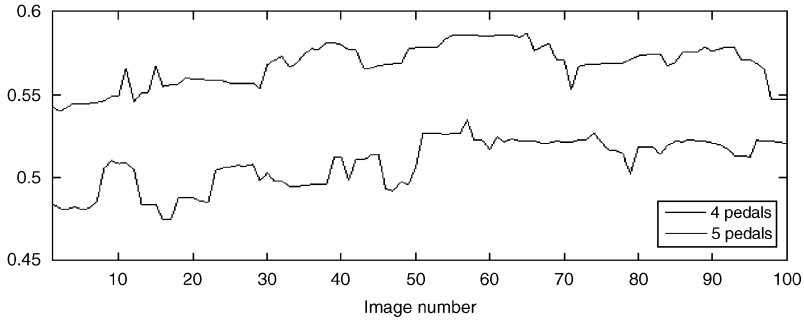

Fig. 10. Plot of the first F_1 feature for all 4-petal and 5-petal images.

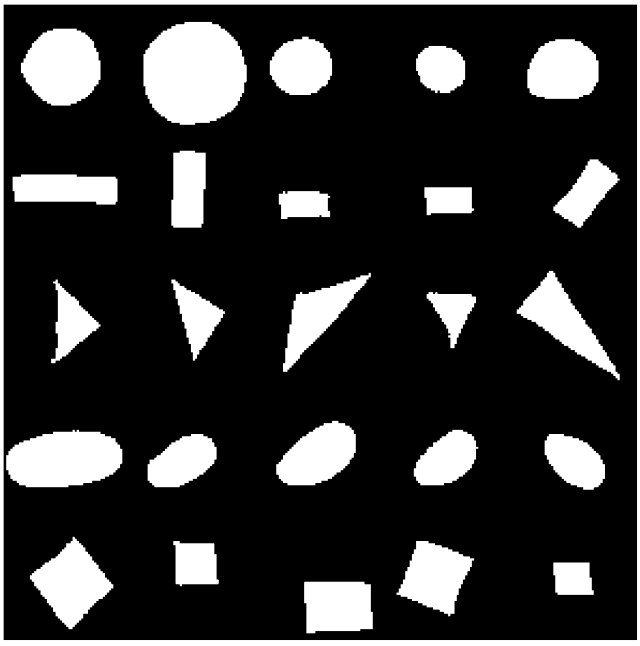

Fig. 11. Samples of the hand-drawn shapes.

Table 2
Correct classification rates of simple shapes using different number of features from F_1, F_2, and F_3 sets

n	F_1 features (%)	F_2 features (%)	F_3 features (%)
4	96.0	96.8	96.0
8	99.2	98.4	97.6
12	95.2	95.2	96.8
16	97.6	97.2	98.4
20	97.6	99.2	98.4

5.2. N-petal images

We generated five sets of 100 n-petal images for $n = 3$–7 (total of 500 images) using Eq. (19). For each set, the variable a was randomly chosen between 1 and 2 and ε was randomly chosen between 0 and 1. This created a lot of variation in the images from a particular class and made images from some classes look similar to images from other classes. Sample images are shown in Fig. 12 . The three sets of features for these images were generated and a group of simple feedforward neural nets with one hidden layer were trained on 60% of the images in the data set (300 images) and tested on the remaining 40% (200 images). The number of features used by the neural nets was varied from 4 to 20. Table 4 summarizes the correct classification results of these nets on the test set. Note that all features performed well (all produced a correct classification rate of at least 90%) and we were able to attain a 97.5% correct classification rate with F_1 features.

Table 3
Classification results of the hand-drawn shapes

	F_1 features	F_2 features	F_3 features
Number of features used	12	12	8
Correct classification rate (%)	94.5	93.5	94.0

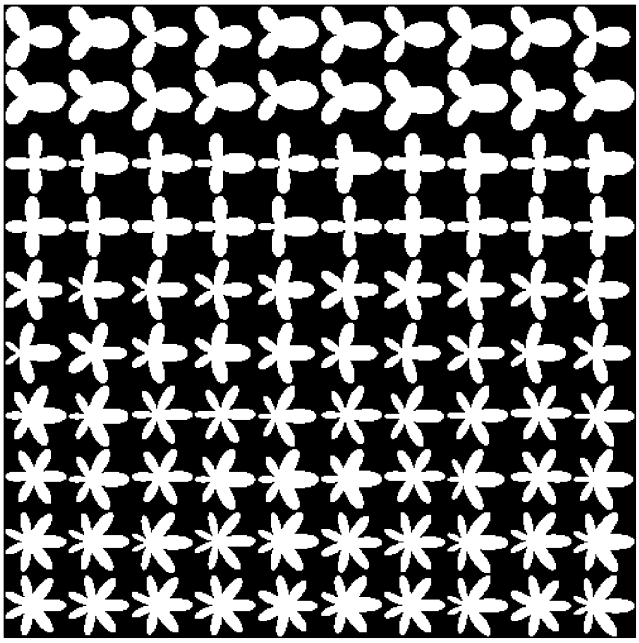

Fig. 12. Sample n-petal images ($n = 3, \ldots, 7$).

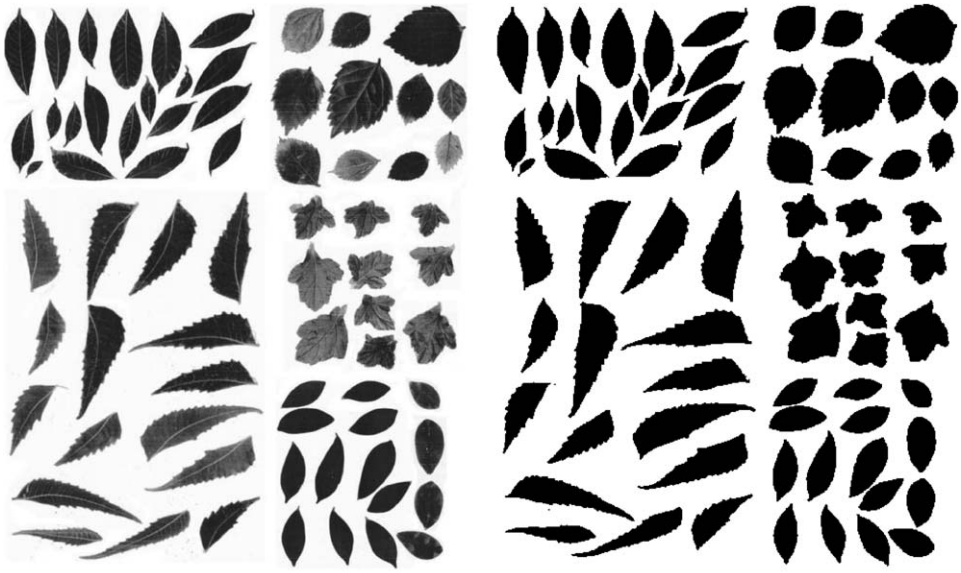

(a) (b)

Fig. 13. Picture of the leaves from five different types of trees: (a) gray-scale; (b) thresholded.

Table 4
Classification results of the n-petal images ($n = 3, \ldots, 7$)

Number of features	F_1 features (%)	F_2 features (%)	F_3 features (%)
4	70.5	65	74.5
8	79.5	83	88.5
12	93	90	92
16	95	89	92
20	97.5	88	94.5

This is another evidence of the robustness/stability of these feature sets, their tolerance of noise and image deformation, and their class separation capability.

5.3. Leaf images

A total of 72 gray-scale images of leaves from five different types of trees were photographed and scanned. The images were thresholded and their F_1, F_2, and F_3 features computed. Fig. 13 shows the gray-scale and thresholded images of the leaves. The average feature vector of the leaves from each class was calculated. These average feature vectors were used as prototypes to represent each of the five leaf classes (one prototype per class). The 72 leaves were classified using the minimum Euclidian distance to the prototypes (the smallest Euclidian distance to a prototype indicates the class to which the image belongs). We varied the number of features used in the classification from 1 to 20. The best classification results using each feature set are shown in Table 5 along with the number of features that allowed such results. As can be seen from the table, correct classification rates of about 89% were achieved using *very few* features (2 or 4) despite the fact that our classifier is very basic and that some leaves from two different classes (upper left and lower right parts of the figure) have very similar shapes and were responsible for many classification errors. A neural network-based classifier would have probably yielded better classification results (due to its non-linear classification boundary capability). However, due to the limited number of samples in this data set, rigorous training and testing of neural networks are not possible.

Table 5
Classification results of leaf images

	F_1 features	F_2 features	F_3 features
Number of features used	2	4	2
Correct classification rate (%)	88.9	84.7	88.9

6. Conclusion

We have studied three sets of features based on the eigenvalues of the Dirichlet Laplacian. These sets of features are translation-, rotation-, and size-invariant. We have shown that the three sets of features were tolerant of boundary noise and deformation and have good inter-class discrimination capabilities. The three sets of features were used successfully to classify natural and man-made images with a high degree of accuracy and using a relatively small number of features (only two features in some cases). We plan to undertake this task of classification using the eigenvalues of the Neumann Laplacian (or free membrane) in further studies. Future work also includes using finite elements method to compute these eigenvalues and an extension of this work to gray-scale images.

7. Summary

We have proposed and studied three sets of features for shape recognition and classification in binary images. The features are based on the eigenvalues of the Dirichlet Laplacian and are translation-, rotation-, and size-invariant. We conducted experiments using computer-generated images that showed the three feature sets were robust, tolerant to boundary noise and deformation, and have good inter-class discrimination capabilities. The three sets of features were used successfully to classify hand-drawn shapes with an average correct classification rate of 94%; synthetic n-pedal images with a correct classification rate ranging from 90% to 97.5%; and natural images of leaves with a correct classification rate of almost 89%. The classification was done using few features (only two features in some cases) and simple feedforward neural networks or minimum Euclidian distance.

References

[1] L. Zusne, Visual Perception of Form, Academic Press, New York, 1970.
[2] H.W. Hake, Form discrimination and the invariance of form, in: L. Uhr (Ed.), Pattern Recognition: Theory, Experiments, Computer Simulations, and Dynamic Models of Form, Perception, and Discovery, Wiley, New York, 1966, pp. 142–173.
[3] D.O. Hebb, The Organization of Behavior, Wiley, New York, 1949.
[4] J.J. Gibson, The Perception of the Visual World, Houghton, Boston, MA, 1950.
[5] D. Marr, A theory for cerebral neocortex, Proc. R. Soc. London B 176 (1970) 161–234.
[6] F. Attneave, Some informational aspects of visual perception, Psychol. Rev. 61 (1954) 183–193.
[7] D.D. Hoffman, W.A. Richards, Parts of recognition, Cognition 18 (1984) 65–96.
[8] A. Pentland, Fractal-based description of natural scenes, IEEE Trans. PAMI 6 (1984) 661–674.
[9] H. Blum, Biological shape and visual science (Part I), J. Theor. Biol. 38 (1973) 205–287.
[10] T. Pavlidis, A review of algorithms for shape analysis, Comput. Graphics Image Process. 7 (1978) 243–258.
[11] D.G. Lowe, Three dimensional object recognition from single two dimensional images, Artif. Intell. 31 (1987) 355–395.
[12] S. Loncaric, A survey of shape analysis techniques, Pattern Recognition 31 (1998) 983–1001.
[13] M. Kac, Can one hear the shape of a drum?, Am. Math. Mon. 73 (1966) 1–23.
[14] M.H. Protter, Can one hear the shape of a drum? revisited, SIAM Rev. 29 (1987) 185–197.
[15] C. Gordon, D. Webb, S. Wolpert, One cannot hear the shape of a drum, Bull. Am. Math. Soc. 27 (1992) 134–138.
[16] M. Zuliani, C. Kenney, S. Bhagavathy, B.S. Manjunath, Drums and Curve Descriptors, UCSB Visition Research Lab Preprint, 2004 ⟨http://vision.ece.ucsb.edu/publications/04BMVCMarco.pdf⟩.
[17] T.A. Driscoll, Eigenmodes of isospectral drums, SIAM Rev. 39 (1997) 1–17.
[18] G.E. Forsythe, Asymptotic lower bounds for the fundamental frequency of convex membranes, Pac. J. Math. 5 (1955) 691–702.
[19] G.E. Forsythe, Asymptotic lower bounds for the frequencies of certain polygonal membranes, Pac. J. Math. 4 (1954) 467–480.
[20] L. Fox, P. Henrici, C. Moler, Approximations and bounds for eigenvalues of elliptic operators, SIAM. J. Numer. Anal. 4 (1967) 89–102.
[21] I. Fried, M. Chavez, Superaccurate finite element eigenvalue computation, J. Sound Vib. 275 (2004) 415–422.
[22] P. Grinfeld, G. Strang, The Laplacian eigenvalues of a polygon, Comput. Math. Appl. 48 (2004) 1121–1133.
[23] M.K. Jain, Numerical Solution of Differential Equations, Wiley, New York, 1979.
[24] I.W. Knowles, M.L. McCarthy, Isospectral membranes: a connection between shape and density, J. Phys. A 37 (2004) 8103–8109.
[25] J.R. Kuttler, V.G. Sigillito, Eigenvalues of the Laplacian in two dimensions, SIAM Rev. 26 (2) (1984) 163–193.
[26] L.M. Cureton, J.R. Kuttler, Eigenvalues of the Laplacian on regular polygons and polygons resulting from their dissection, J. Sound Vib. 220 (1999) 83–98.
[27] J.R. Kuttler, A fourth-order finite difference approximation for the fixed membrane eigenproblem, Math. Comput. 25 (1971) 237–256.
[28] J.R. Kuttler, Finite difference approximations for eigenvalues of uniformly elliptic operators, SIAM J. Numer. Anal. 7 (1970) 206–232.
[29] G. Pólya, Sur une interprétation de la méthode des différences finies qui peut fournir des bornes supérieures ou infrieures, C. R. Acad. Sci. Paris 235 (1952) 995–997 (Reprinted as J. Hersch, G.-C. Rota (Eds.), George Pólya: Collected Papers, vol. III: Analysis, MIT Press, Cambridge, MA, 1984, pp. 284–286 with comments by J. Hersch, G. Strang, p. 511).
[30] G. Pólya, Estimates for Eigenvalues, in: Studies in Mathematics and Mechanics Presented to Richard von Mises, Academic Press, New York, 1954, pp. 200–207, (Reprinted as J. Hersch, G.-C. Rota (Eds.), George Pólya: Collected Papers, vol. III: Analysis, MIT Press, Cambridge, MA, 1984, pp. 394–401 with comments by J. Hersch, p. 515).
[31] G.J. Fix, G. Strang, An Analysis of the Finite Element Method, Prentice-Hall, Englewood Cliffs, NJ, 1973.
[32] J.C. Strikwerda, Finite Difference Schemes and Partial Differential Equations, Wadsworth & Brooks/Cole, Pacific Grove, 1989.
[33] H.F. Weinberger, Upper and lower bounds for eigenvalues by finite difference methods, Commun. Pure Appl. Math. 9 (1956) 613–623.
[34] H.F. Weinberger, Lower bounds for higher eigenvalues by finite difference methods, Pac. J. Math. 8 (1958) 339–368;
erratum, 941.
[35] L.E. Payne, G. Pólya, H.F. Weinberger, On the ratio of consecutive eigenvalues, J. Math. Phys. 35 (1956) 289–298 (Reprinted as J. Hersch, G.-C. Rota (Eds.), George Pólya: Collected Papers, vol. III: Analysis, MIT Press, Cambridge, MA, 1984, pp. 420–429 with comments by J. Hersch, p. 521).
[37] M.S. Ashbaugh, The universal eigenvalue bounds of Payne–Pólya–Weinberger, Hile-Protter, and H.C. Yang, in: Spectral and inverse spectral theory (Goa, 2000), Proc. Indian Acad. Sci. Math. Sci. 112 (2002) 3–30.
[38] M.S. Ashbaugh, Isoperimetric and universal inequalities for eigenvalues, in: E.B. Davies, Yu. Safarov (Eds.), Spectral Theory and Geometry, London Mathematical Society Lecture Series, vol. 273, Cambridge University Press, Cambridge, 1999, pp. 95–139.
[39] G.N. Hile, M.H. Protter, Inequalities for eigenvalues of the Laplacian, Indiana Univ. Math. J. 29 (1980) 523–538.
[40] H.C. Yang, Estimates of the difference between consecutive eigenvalues, 1995, preprint (revision of International Centre for Theoretical Physics preprint IC/91/60, Trieste, Italy, April 1991).
[41] I. Chavel, Eigenvalues in Riemannian Geometry, Academic Press, New York, 1984.
[42] In: M. Abramowitz, I.A. Stegun (Eds.), Handbook of Mathematical Functions, National Bureau of Standards Applied Mathematics Series, vol. 55, US Government Printing Office, Washington, DC, 1964.
[43] M.S. Ashbaugh, R.D. Benguria, Proof of the Payne–Pólya–Weinberger conjecture, Bull. Am. Math. Soc. 25 (1991) 19–29.
[44] A.D. Melas, The stability of some eigenvalue estimates, J. Differ. Geom. 36 (1992) 19–33.

[45] R. Courant, D. Hilbert, Methods of Mathematical Physics, second ed., Interscience Publishers, New York, 1965.
[46] C. Felippa, 50 year classic reprint: an appreciation of R. Courant's "Variational methods for the solution of problems of equilibrium and vibrations" [Bull. Am. Math. Soc. 49 (1943), 1–23], Int. J. Numer. Methods Eng. 37 (1994) 2159–2187.
[47] A. Weinstein, Some numerical results in intermediate problems for eigenvalues, in: J.E. Bramble (Ed.), Numerical Solution of Partial Differential Equations, Academic Press, New York, 1966, pp. 167–191.
[48] H.W. Weinberger, Variational Methods for Eigenvalue Approximation, SIAM, Philadelphia, 1970.
[49] F.H. Hilderbrand, Finite-Difference Equations and Simulations, Prentice-Hall, Englewood Cliffs, NJ, 1968.

Further reading

[36] J. Hersch, G.-C. Rota (Eds.), George Pólya: Collected Papers, vol. III: Analysis, MIT Press, Cambridge, MA, 1984.

About the Author—MOHAMED A. KHABOU got his Ph.D. in electrical engineering from University of Missouri, Columbia in 1999. He is currently an assistant professor in the Department of Electrical and Computer Engineering at University of West Florida. Dr. Khabou's research interests include automatic target recognition, handwriting recognition, human face detection/recognition, artificial neural networks, mathematical morphology, regularization theory, entropy optimization, and fuzzy logic. He is an IEEE senior member.

About the Author—LOTFI HERMI obtained his Ph.D. in Mathematics from the University of Missouri, Columbia in 1999. He is currently a visiting assistant professor in the Department of Mathematics at the University of Arizona. Dr. Hermi is interested in spectral bounds for eigenvalues of elliptic operators and their applications to image recognition. He is a member of the AMS.

About the Author—MOHAMED B.H. RHOUMA received the degree of Ingenieur Principal in industrial engineering from the Ecole Nationale d'Ingenieurs de Tunis, Tunisia in 1989 and both his MSc and Ph.D. in Mathematics from the University of Missouri, Columbia in 1995 and 1999, respectively. He did his postdoctoral training at the Center for Dynamical Systems and Nonlinear Studies at Georgia Institute of Technology in Atlanta. He is currently an assistant professor of Mathematics at Sultan Qaboos University in Oman. Dr Rhouma's main area of research is dynamical systems and their applications in pattern recognition. Dr Rhouma is a member of the AMS and SIAM.